scientific reports

Check for updates

OPEN

Comprehensive analysis of lipid metabolic signatures identified CEBPD promotes breast cancer cell proliferation

Yu Zhao[1], Huan He[1], Linyan Huang[1] & Linna Yu[1,2]✉

Breast cancer (BRCA) remains the leading cause of cancer-related mortality worldwide, with lipid metabolism emerging as a critical factor in tumor progression that influences cell proliferation, migration, and immune response. Insights into lipid metabolism signatures and associated genes may offer new prognostic and therapeutic avenues. In this study, we leveraged scRNA-seq and bulk transcriptome data to assess the expression patterns and prognostic significance of lipid metabolism-related genes in BRCA. Through single-cell transcriptomic analysis of primary BRCA samples, we identified a specific set of lipid metabolism signature genes and constructed a prognostic risk model based on these signatures. This model enables patient stratification by risk scores, supporting an integrated analysis of lipid metabolism, immune landscape, and clinical outcomes. Importantly, we identified CEBPD, ABCA1, and CYP27A1 as independent prognostic genes linked to lipid metabolism, with functional assays revealing an inhibitory role for CEBPD in BRCA cell proliferation. Our findings underscore the influence of adipocytes in BRCA progression and propose CEBPD as a potential target for therapeutic intervention. This study provides a foundation for further exploration of metabolism-based strategies to enhance BRCA outcomes.

Keywords BRCA, Adipocytes, Single-cell sequencing, CEBPD, Cell proliferation

Breast cancer (BRCA) is one of the most prevalent cancers worldwide and represents a significant cause of cancer-related mortality among women evidence indicates that the tumor microenvironment, particularly components such as immune cells and adipocytes, plays a crucial role in BRCA progression and therapeutic response[1–3]. Adipondant in breast tissue, produce numerous cytokines, growth factors, and metabolic substrates that influence tumor biology[4,5]. The role of lipid metabolism in supportingwth has garnered increasing interest, with lipid-related pathways shown to impact cell proliferation, metastasis, and drug resistance in various cancers[6,7].

By integrating scRNA-seq with transcriptomic data, researchers can identify metabolic dependencies and their interactions with tumor cells, as well as prognostic markers specific to BRCA subtypes[8,9]. Through scRNA-seq, researchers can identify distinct cell populationsimmune cells, fibroblasts, and adipocytes, that contribute to the complex tumor microenvironment in BRCA[1,10]. Recent advancements have highlighted the potential of scRNA-seq to elucidate sabolic dependencies in these distinct cell types and their interactions with tumor cells[11,12]. Recent studies have sholism in the tumor microenvironment is closely linked to cancer aggressiveness and poor prognosis[13,14]. However, the specific contributions of lipid metabolism-related genes, particularly their role in BRCA prognosis, remain underexplored.

In this study, we leveraged scRNA-seq and transcriptomic data to examine the expression and prognostic significance of lipid metabolism-associated genes in BRCA. Through single-cell transcriptomic profiling of primary BRCA samples, we identified a set of lipid metabolism signature genes and developed a prognostic risk model based on these signatures. This model stratifies patients by risk score, enabling a deeper understanding of the interplay between lipid metabolism, immune status, and clinical outcomes. Notably, we identified CEBPD, ABCA1, and CYP27A1 as independent prognostic genes linked to lipid metabolism, with functional validation demonstrating an inhibitory effect of CEBPD on BRCA cell proliferation.

[1]People's Hospital of Qianxinan Prefecture, Xingyi, Guizhou, China. [2]Key Laboratory of Drug Quality Control and Pharmacovigilance (Ministry of Education), State Key Laboratory of Natural Medicines, Department of Pharmaceutics, NMPA Key Laboratory for Research and Evaluation of Pharmaceutical Preparations and Excipients, China Pharmaceutical University, Nanjing 210009, China. ✉email: yulinna8941@163.com

Materials and methods

Data collection

Transcriptomic and clinical data for breast cancer, encompassing 1,092 tumor samples and 113 normal controls, were sourced from the Cancer Genome Atlas (TCGA) (https://portal.gdc.cancer.gov/, accessed September 9, 2024). Clinical parameters included survival time, survival status, age, sex, and TNM stage. Additionally, single-cell RNA sequencing data for six primary breast cancer samples were obtained from the GSE263995 and GSE248288 datasets[15,16].

Single-cell sequencing analysis

Data from both datasets were processed using the Seurat package for quality control and clustering, leveraging dimensionality reduction techniques such as principal component analysis (PCA) and t-SNE. Differentially expressed genes (DEGs) between groups were identified using the "FindMarkers" function in Seurat, with statistical significance assessed by the Wilcoxon test (p.adj < 0.05) and default settings applied[17]. Cell types were annotated using the SingleR package to determine key gene markers[18].

Cell-cell communication and pseudotime analysis

Ligand-receptor interactions within the single-cell RNA sequencing data were analyzed using the CellChat package, identifying potential signaling pathways based on ligand-receptor expression across cell subtypes[19]. Cell differentiation trajectories were inferred with Monocle 3[20], an unsupervised approach that orders cells along trajectories representing biological processes, such as cell differentiation in this study.

Construction of prognostic risk score model

Key prognostic genes were identified through univariate Cox regression, followed by construction of a risk score model using Lasso regression. Each patient's risk score was calculated to evaluate its prognostic value for breast cancer. Kaplan-Meier survival analyses compared high- and low-risk groups, with differential gene expression visualized via heat maps. Predictive performance was assessed using receiver operating characteristic (ROC) curves, and nomograms were developed to estimate 3-, 5-, and 8-year survival probabilities. Model accuracy was verified with calibration curves.

Functional enrichment and protein-protein interaction network analysis

Functional enrichment of recurrence-related or cell communication DEGs was performed using DAVID (v6.8, https://david.ncifcrf.gov/, accessed September 9, 2024)[21], where the KEGG database was referenced from Kanehisa laboratory[22]. Protein-protein interaction (PPI) networks were constructed using the STRING database (v11.0, https://string-db.org, accessed September 9, 2024)[23].

Evaluation of immune status, immunotherapy response, and genomic heterogeneity

Immune cell infiltration and overall immune scores for each breast cancer patient were quantified using ESTIMATE, EPIC, and Timer algorithms to compare differences between high- and low-risk groups[24,25]. Microsatellite instability (MSI) and tumor mutation burden (TMB) were analyzed to evaluate immunotherapy responsiveness across risk groups. Additionally, tumor stage data from the TCGA-LIHC cohort were analyzed to compare risk score distributions.

Protein structure prediction and mutation analysis

Protein structure predictions were conducted by uploading gene symbols to Genecard (https://www.genecards.org/, accessed September 9, 2024). Somatic mutation and copy number variation (CNV) profiles were acquired from the TCGA data portal (https://portal.gdc.cancer.gov/, accessed September 9, 2024). Visualization of somatic mutation and CNV data was achieved using the R package "maftools"[26]. Significant CNV amplifications or deletions were identified using GISTIC 2.0 with a threshold of FDR Q < 0.05.

Cell culture and transfection

Breast cancer cell lines, kindly provided by Professor Jie Chen of Zunyi Medical University[27], were maintained at 37 °C in a humidified atmosphere with 5% CO_2. Cells were cultured in RPMI-1640 medium for BT474 and SKBR3 lines and in DMEM for MCF-7, each supplemented with 10% fetal bovine serum (FBS, Gibco) and 1% penicillin-streptomycin (PS, Invitrogen). Synthetic siRNA (Santa Cruz, sc-37722) or control siRNA (Santa Cruz, sc-37007) was incubated with Lipofectamine® RNAiMAX (Life Technologies) in DMEM/RPMI-1640 containing 10% FBS at room temperature for 20 min. Cells were treated with 30 nM siRNA and incubated for 48 h. Specifically, the siRNA of FBXW7 was synthesized by Qingke Biotechnology with the following sequence: F: UCACAUUCUCCUCUUUUCCUC; R: GGAAAAGAGGAGAAUGUGAAA.

Real-time quantitative PCR (RT-qPCR)

RT-qPCR was conducted following the protocol described by Wang et al.[28]. Cells were washed with PBS, and RNA was extracted and purified using the RNeasy® Mini Kit (Qiagen) according to the manufacturer's protocol. Reverse transcription into cDNA was carried out using the iScript cDNA Synthesis Kit (Bio-Rad). PCR amplification was conducted with Fast SYBR Green Master Mix (Bio-Rad), using GAPDH as the reference gene. Relative gene expression levels were calculated using the 2-ΔΔCt method. Primer sequences used were as follows: CEBPD: Forward: 5′-CGCAGACAGTGGTGAGCTT-3′, Reverse: 5′-CTTCTGCTGCATCTCCTGGT-3′; FBXW7: Forward: 5′- GTTTGGTCAGCAGTCACAGGCA-3′, Reverse: 5′- CCACACTTTGAGTGTCCGATCTG-3′; GAPDH: Forward: 5′-GCCTCGTCTCATAGACAAGATG-3′, Reverse: 5′-CAGTAGACTCCACGACATAC-3′.

Colony formation assay

To assess long-term cell viability, 48 h after siRNA transfection, 1000 breast cancer cells were seeded into 6-well plates and cultured for two weeks. Cells were subsequently fixed with 4% paraformaldehyde for 15 min and stained with 0.5% (w/v) crystal violet (Sigma-Aldrich). Colonies were scanned using an Odyssey scanner (LI-COR, Lincoln, NE) and quantified with ImageJ software.

Cell viability assay

Cell viability was evaluated 48 h post-transfection using the Cell Counting Kit-8 (CCK-8) assay (MedChem Express, Monmouth Junction, NJ). Cells were seeded in 96-well plates at a density of 2 × 10^4 cells per well and incubated for 12 h. Following this, 100 µL of basal medium and 10 µL of CCK-8 solution were added to each well and incubated for an additional hour. Absorbance at 450 nm was measured using a microplate reader (Thermo Scientific, Waltham, MA). All assays were performed in triplicate.

Statistical analysis

Group differences were assessed using the Wilcoxon test, and associations were analyzed using Spearman rank correlation. Kaplan-Meier survival curves and log-rank tests were used for survival analysis. Cox regression analysis was conducted with the "survival" package in R to calculate hazard ratios (HRs) and 95% confidence intervals (CIs). All statistical tests were two-sided, with significance defined at $P < 0.05$. Statistical analyses were performed using R software (version 4.2.2).

Results

Single-cell analysis of breast cancer

We analyzed single-cell sequencing data from six breast cancer samples obtained from two datasets, performing quality control to remove non-viable cells (Fig. 1A). Using the "Seurat" package, we identified the top 2,000 highly variable genes, revealing significant cell-to-cell expression variability essential for accurate cell-type identification (Fig. 1B and C). Dimensionality reduction using principal component analysis (PCA) and t-SNE classified the samples into 21 distinct cell clusters (Fig. 1D). Differentially expressed genes were visualized through volcano plots, with the top 10 heterogeneous genes mapped to a t-SNE plot showing cluster-specific expression (Fig. 1E and F). Further annotation revealed six major cell types: adipocytes, epithelial cells, macrophages, endothelial cells, fibroblasts, and T cells (Fig. 1G).

Identification of lipid metabolism-related genes and cell communication analysis

Adipocyte-specific genes were compiled as the "Adipocytes" list, while 776 genes involved in lipid metabolism were collected as the "Metabolism" list based on prior research[29]. From these, 81 breast cancer lipid metabolism-related genes were extracted (Fig. 2A). Gene Ontology (GO) analysis indicated that these genes are predominantly associated with the endoplasmic reticulum membrane, extracellular exosomes, and extracellular regions, and are involved in lipid metabolism and inflammatory responses, with functions including iron ion binding, heme binding, and fatty acid binding (Fig. 2B). KEGG pathway enrichment analysis further showed strong associations with metabolic pathways, PPAR signaling, and arachidonic acid metabolism (Fig. 2C). A protein-protein interaction network for these genes, generated through the STRING database, identified FASN as the central gene, as suggested by three cytohub algorithms (Fig. 2D-G).

To investigate adipocyte communication in breast cancer, we used the CellChat package to infer the number and strength of intercellular communication networks (Fig. 2H-I). Adipocytes and T cells displayed the fewest interactive signals for both input and output. Interestingly, fibroblasts exhibited significantly more output than input signals (Fig. 2J). Further analysis revealed that macrophages had the highest level of communication with adipocytes, primarily through HLA-CD4 signaling pathways (Fig. 2K).

Constructing risk scores based on lipid metabolism signature genes using the LASSO-Cox algorithm

To identify lipid metabolism-related genes associated with prognosis, we conducted a univariate survival analysis on 81 differentially expressed genes, identifying 10 genes with significant prognostic associations ($P < 0.05$) (Fig. 3A). In addition, we used LASSO-Cox regression to screen for variables significantly associated with OS. The curves of the regression coefficient versus log (λ) and the partial likelihood deviation versus log (λ) were used to screen 13 independent prognostic genes associated with OS when lambda.1se represented the optimal lambda, to construct a prognostic risk score model (Fig. 3B and C):

$$\text{RiskScore} = 0.0109\times\text{IDI1} - 0.0574\times\text{PLA2G2D} + 0.0297\times\text{ABCA1} - 0.0544\times\text{SLC27A2} + 0.0117\times\text{SQLE} - 0.0427\times\text{FABP7} + 0.0781\times\text{LGMN} - 0.0384\times\text{HSD11B1} - 0.0259\times\text{SMARCD3} - 0.0926\times\text{CEBPD} + 0.0181\times\text{BCHE} - 0.1119\times\text{CYP27A1} + 0.0014\times\text{MGLL}.$$

Heatmap analysis showed that genes PLA2G2D, SLC27A2, FABP7, HSD11B1, CEBPD, and CYP27A1 were negatively correlated with the risk score, while the remaining genes displayed positive correlations (Fig. 3D). Kaplan-Meier survival analysis indicated significantly lower survival rates in the high-risk group compared to the low-risk group (Fig. 3E). The model's prognostic accuracy, evaluated via ROC analysis, demonstrated AUC values of 0.69, 0.70, and 0.71 for 3-, 5-, and 8-year survival, respectively (Fig. 3F). A nomogram integrating clinical parameters with risk scores was developed to predict 1-, 3-, and 5-year survival outcomes (Fig. 3G). Kaplan-Meier analysis showed that patients with higher nomogram scores had a significantly worse prognosis (Fig. 3H). Further ROC analysis yielded AUC values of 0.84, 0.83, and 0.80 for 3-, 5-, and 8-year survival, respectively (Fig. 3I). Calibration curves confirmed the model's robustness in predictive accuracy (Fig. 3J).

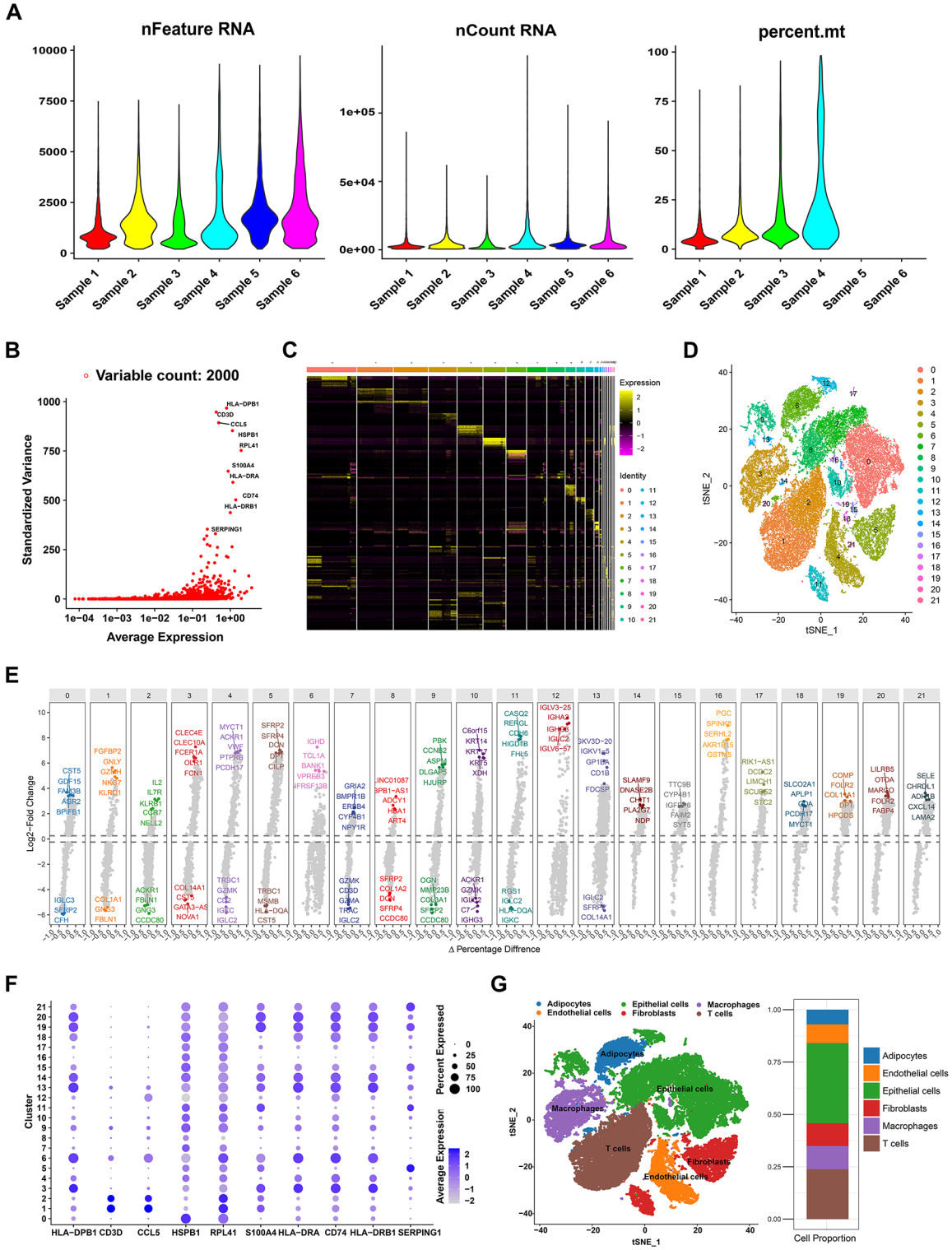

Fig. 1. Analysis of single-cell transcriptome data to identify lipid metabolism signature genes in breast cancer. (**A**) Cell quality control before dimensionality reduction analysis. (**B**) Volcano plot shows the top 3000 highly variable genes. (**C**) Heat map shows the expression of key differential genes in different clusters. (**D**) PCA and t-SNE dimensionality reduction divide cells into 21 different clusters. (**E**) Volcano plot shows the key differential genes in 21 cell clusters. (**F**) Bubble plot shows the expression distribution of TOP10 heterogeneous genes in 21 different cell clusters. (**G**) Cell annotation using the SingleR package divides cells into 6 main clusters. On the left is a t-SNE 2D plot colored by cell type, and on the right is the content of each cell.

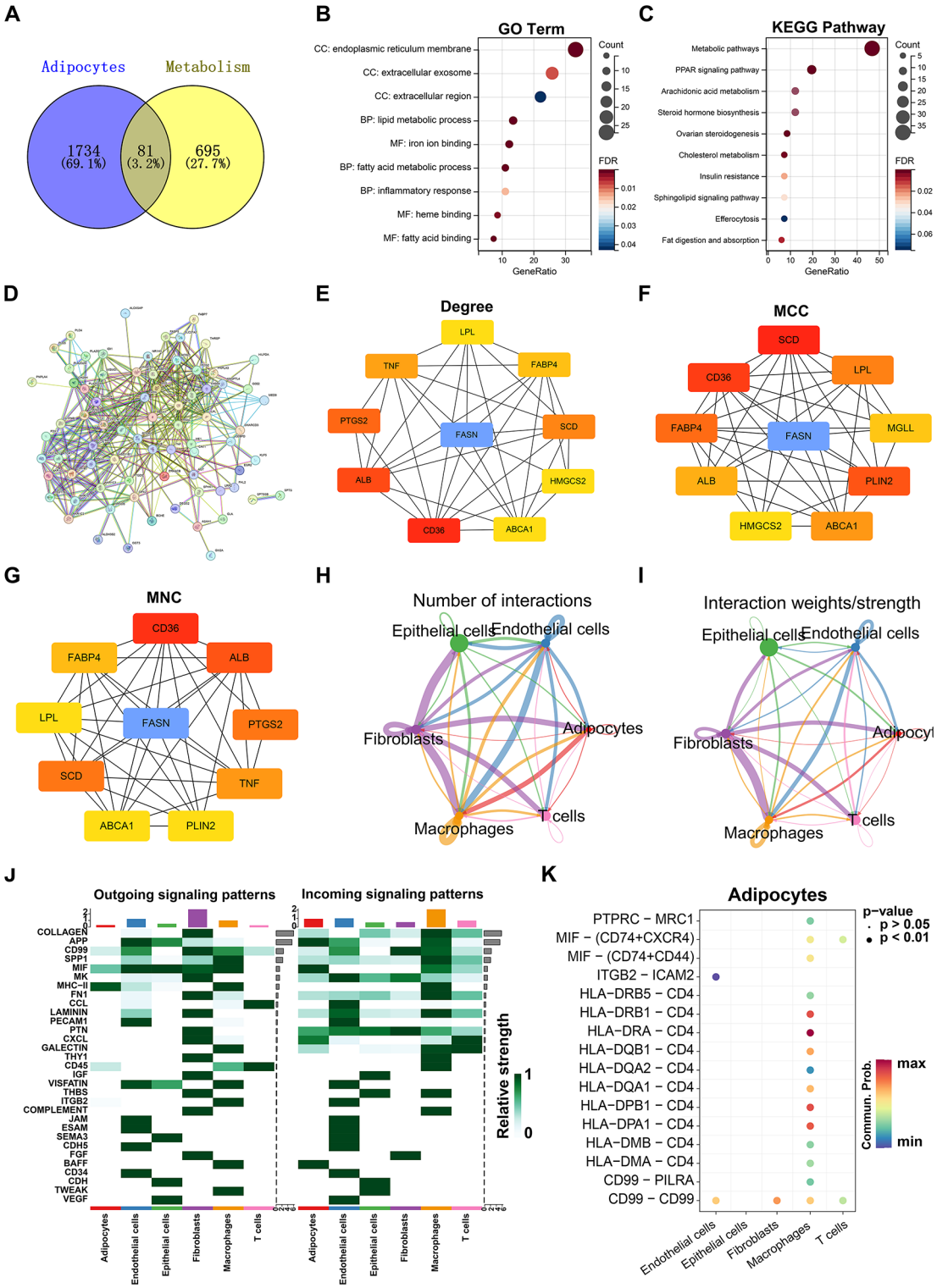

Fig. 2. Extraction of lipid metabolism characteristic genes and intercellular communication. (**A**) Venny plot of characteristic gene list of adipocytes and metabolic gene set in GSEA. (**B**) GO analysis of 81 lipid metabolism characteristic genes. (**C**) KEGG analysis of 81 lipid metabolism characteristic genes. (**D**) Protein interaction network of 81 lipid metabolism characteristic genes. (**E**) Degree algorithm calculates hub proteins of 81 lipid metabolism proteins. (**F**) MCC algorithm calculates hub proteins of 81 lipid metabolism proteins. (**G**) MNC algorithm calculates hub proteins of 81 lipid metabolism proteins. (**H**) Intercellular communication between 6 cell types, thickness indicates the number of communications. (**I**) Intercellular communication between 6 cell types, thickness indicates the communication intensity. (**J**) Output and input model characteristics of 6 cell types. (**K**) Distribution of communication models between adipocytes and other cells.

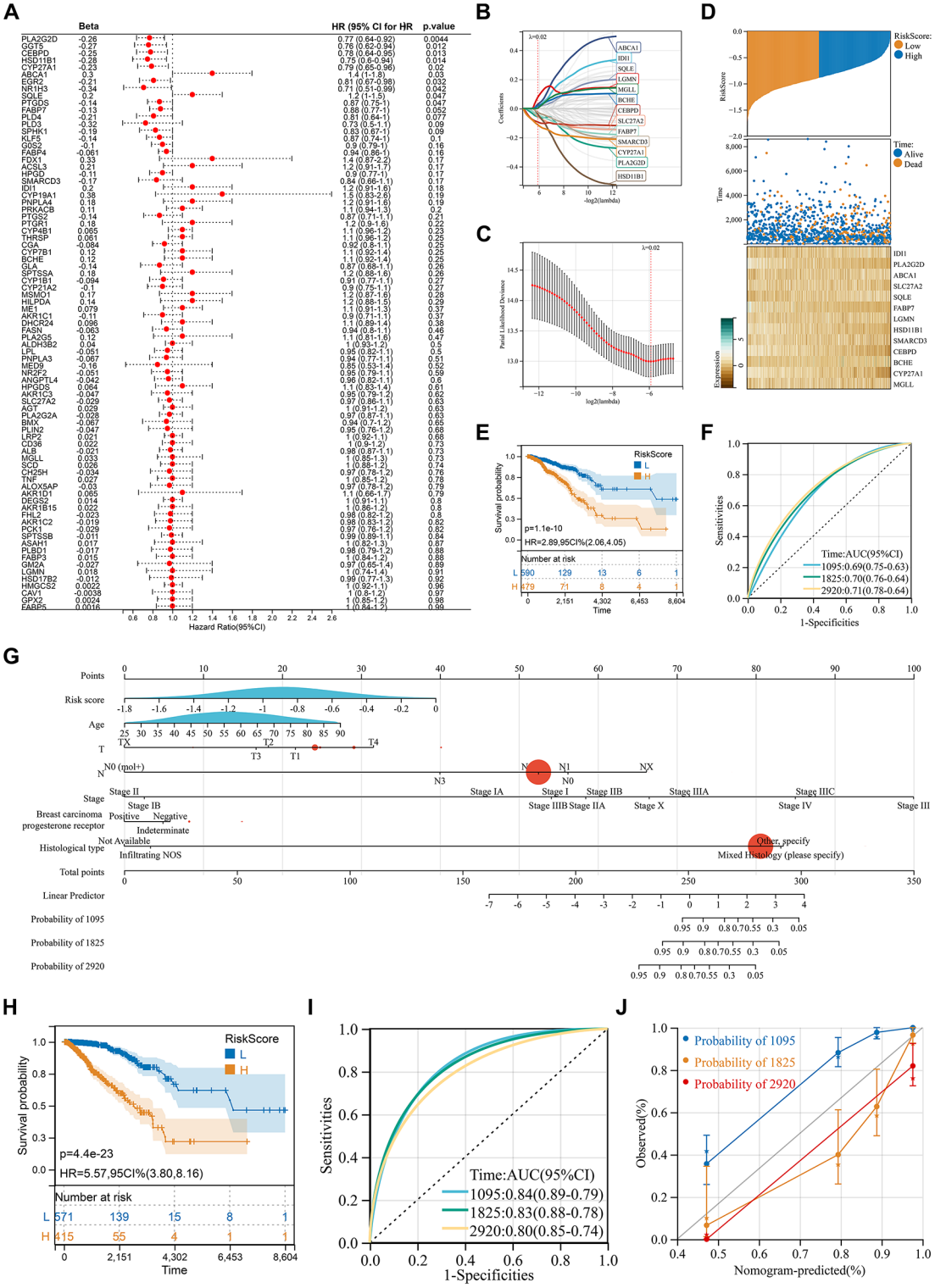

Fig. 3. Risk score model developed using LASSO algorithm and integrated with clinical parameters. (**A**) Univariate Cox analysis identified 10 prognostic genes. (**B**,**C**) Gene selection using LASSO-Cox algorithm to build the best model. (**D**) Expression pattern of 13 risk score genes and relationship with survival time. (**E**) Kaplan-Meier analysis showed that the high-risk group had a worse prognosis than the low-risk group. (**F**) ROC curve analysis showed the AUC values of the risk score model at 1, 3, and 5 years. (**G**) Nomogram integrating risk score and clinical factors to predict 1, 3, and 5-year survival. (**H**) Kaplan-Meier analysis showed that patients with higher nomogram scores had a worse prognosis. (**I**) ROC curves showed the AUC values of the nomogram scores at 1, 3, and 5 years. (**J**) Calibration curves showed the accuracy of the model in predicting patient survival.

Immune landscape, tumor stemness, and genomic heterogeneity under risk score grouping

To assess the relationship between risk score and immune status, immune scores for each sample were calculated using the Estimate algorithm. Spearman correlation analysis revealed that the risk score was negatively correlated with both the immune score and Estimate score but showed no correlation with the stromal score (Fig. 4A). Immune cell infiltration across different risk groups was then evaluated using the Timer and EPIC algorithms, showing significant differences in the infiltration of B cells, T cells, endothelial cells, neutrophils, and fibroblasts, while macrophage and NK cell infiltration remained similar between groups (Fig. 4B and C). Risk scores were also found to increase with tumor stage (Fig. 4D) but showed no correlation with MSI and TMB scores (Fig. 4E and F). The TIDE algorithm indicated that patients predicted to respond to immunotherapy exhibited higher risk scores (Fig. 4G). Specifically, high-risk patients demonstrated lower TIDE, dysfunction, and CAF scores, yet had elevated exclusion and MDSC scores (Fig. 4H).

Expression and prognostic analysis of risk score genes

To clarify the prognostic role of risk score genes in breast cancer, we conducted Kaplan-Meier (KM) survival analysis on ten genes identified by univariate Cox analysis (Fig. 5A). High expression levels of ABCA1 and SQLE were linked to poorer prognosis, while elevated expression of other genes—except GGT5—was associated with improved prognosis. Single-cell t-SNE heatmaps showed distinct expression patterns for these ten genes, with CEBPD showing the highest expression, PLA2G2D the lowest, and ABCA1 and CYP27A1 exhibiting highly similar expression profiles (Fig. 5B). Additionally, pseudo-time analysis was performed to investigate the developmental role of lipid metabolism signature genes in breast cancer cells (Fig. 5C). After arranging all cells by pseudo-time (Fig. 5D), adipocyte development was specifically examined (Fig. 5E). In overall cell development, VIM, SPARCL1, and IGFBP7 emerged as key signature genes (Fig. 5F), while CEBPD, a lipid metabolism gene of interest, demonstrated relevance to developmental stages (Fig. 5G and H), including in adipocyte differentiation.

CEBPD, a proliferation-associated independent prognostic factor in breast cancer

Six risk-associated genes were identified from LASSO and univariate Cox regression analyses (Fig. 6A). Multivariate Cox regression analysis further confirmed that CEBPD, ABCA1, and CYP27A1 serve as independent prognostic factors in breast cancer (Fig. 6B). Structural analyses of CEBPD, ABCA1, and CYP27A1 revealed protein sizes of 28.4 kDa, 25.4 kDa, and 60.2 kDa, respectively (Fig. 6C-E). In the TCGA cohort, CEBPD and ABCA1 showed reduced expression in tumor tissues (Fig. 6F, G), while CYP27A1 expression did not differ significantly (Fig. 6H). Notably, although ABCA1 was identified as an independent risk gene, its low expression in tumor tissue contrasts with its previously reported tumor-suppressive role in promoting membrane fluidity[30]. Given this, CEBPD was selected for further studies, with siRNA-mediated knockdown confirmed by real-time PCR (Fig. 6I). Initial assays revealed that CEBPD knockdown enhanced MCF-7 cell proliferation in both CCK-8 and colony formation assays (Fig. 6J, K).

Inhibition of nuclear-localized CEBPD promotes breast cancer cell proliferation

Immunofluorescence data from the HPA database showed that CEBPD is predominantly localized within the nucleus (Fig. 7A). TCGA proteomic data revealed no significant difference in CEBPD protein abundance in tumor versus normal tissues (Fig. 7B), although phosphorylation at Y194 was markedly elevated in tumor samples (Fig. 7C). STRING analysis further identified CEBPD's interaction network, which includes proteins involved in cancer pathways, transcriptional dysregulation, and thyroid hormone signaling (Fig. 7D, E). Mutation analysis showed a higher mutation frequency of CDH1 in high-CEBPD expression samples, while lower CEBPD expression correlated with mutations in TP53, GATA3, SORCS3, and FLG (Fig. 7F). To confirm CEBPD's role in cell proliferation across different breast cancer lines, we examined its effect on BT474 and SKBR3 cells. In both cell lines, si-CEBPD enhanced proliferation, as shown in CCK-8 and colony formation assays (Fig. 7G-J), supporting CEBPD's regulatory role in breast cancer proliferation across multiple cell types.

CEBPD promotes breast cancer cell proliferation in a FBXW7-dependent manner

FBXW7 acts as a tumor suppressor in breast cancer and has been reported to be regulated by CEBPD, thereby affecting breast cancer metastasis[31,32]. Here, we used siRNA to inhibit the expression of FBXW7 (verified by real-time fluorescence quantitative PCR) to explore whether the changes in breast cancer cell proliferation caused by CEBPD are dependent on FBXW7 (Fig. 8A). It is certain that si-FBXW7 promoted the proliferation of BT474 and SKBR3 cells, whether it is evidence from CCK-8 or clone formation experiments (Fig. 8B-E). Furthermore, on the basis of inhibiting FBXW7 expression, the pro-proliferation effect of si-CEBPD was abolished, indicating that CEBPD regulates breast cancer cell proliferation and depends on FBXW7 (Fig. 8F-I).

Discussion

In this study, we conducted an in-depth analysis of single-cell sequencing data from primary breast cancer samples, focusing on identifying lipid metabolism-associated genes. High-quality cells were selected, clustered into 21 distinct groups, and annotated into 6 major cell types. From adipocyte signature genes, 81 lipid metabolism-related genes were identified, and a prognostic model was developed using the LASSO-Cox algorithm, demonstrating a significant correlation between risk score, immune status, and patient outcomes. Multivariate Cox regression identified CEBPD, ABCA1, and CYP27A1 as independent prognostic genes. Functional assays further showed that CEBPD regulates the proliferation of MCF-7, BT474, and SKBR3 cells, highlighting its potential role in breast cancer progression.

The AUC values of the ROC curve for 3-, 5-, and 8-year survival prediction of the nomogram in this study reached 0.84, 0.83, and 0.80, respectively, which are better than previous studies[33–36]. One of the genes that

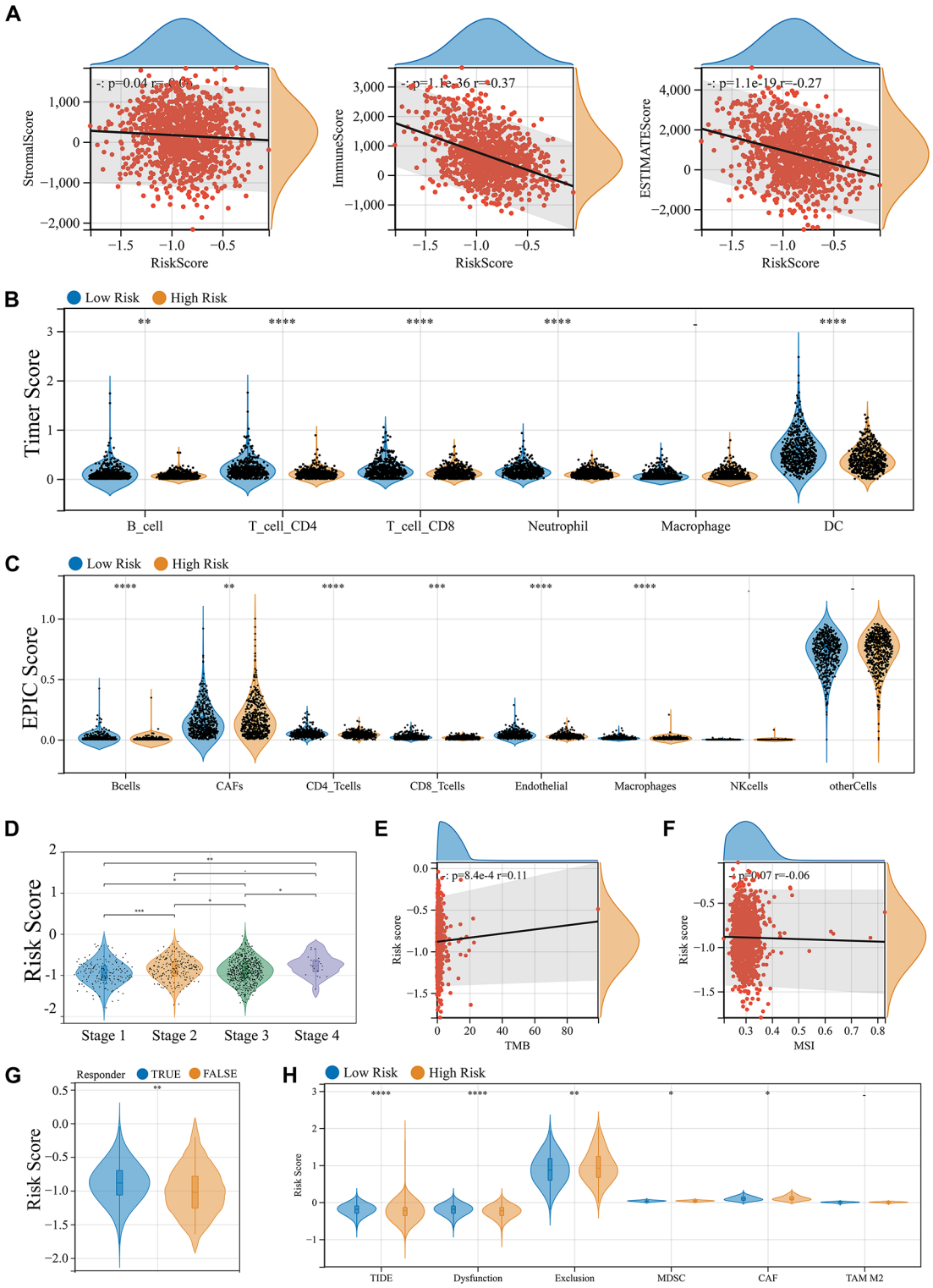

Fig. 4. Evaluation of the relationship between risk score and immune status, immune response, and genomic heterogeneity. (**A**) Correlation analysis between sample immune score assigned by Estimate algorithm and risk score spermman. (**B**) Differences in infiltration of 6 immune cells in different risk groups in TCGA cohort samples evaluated by Timer algorithm. (**C**) Differences in infiltration of 8 immune cells in different risk groups in TCGA cohort samples evaluated by EPIC algorithm. (**D**) Test of risk score differences in different tumor stages. (**E**) Sperman's correlation analysis between TMB score and risk score. (**F**) Sperman's correlation analysis between MSI score and risk score. (**G**) Test of risk score differences between immunotherapy response group and non-response group expected by TIDE algorithm. (**H**) TIDE algorithm evaluates TIDE, dysfunction, exclusion, MDSC, CAP and TAM M2 scores in high-risk and low-risk groups. *indicates $p < 0.05$, **indicates $p < 0.01$, and ***indicates $p < 0.001$.

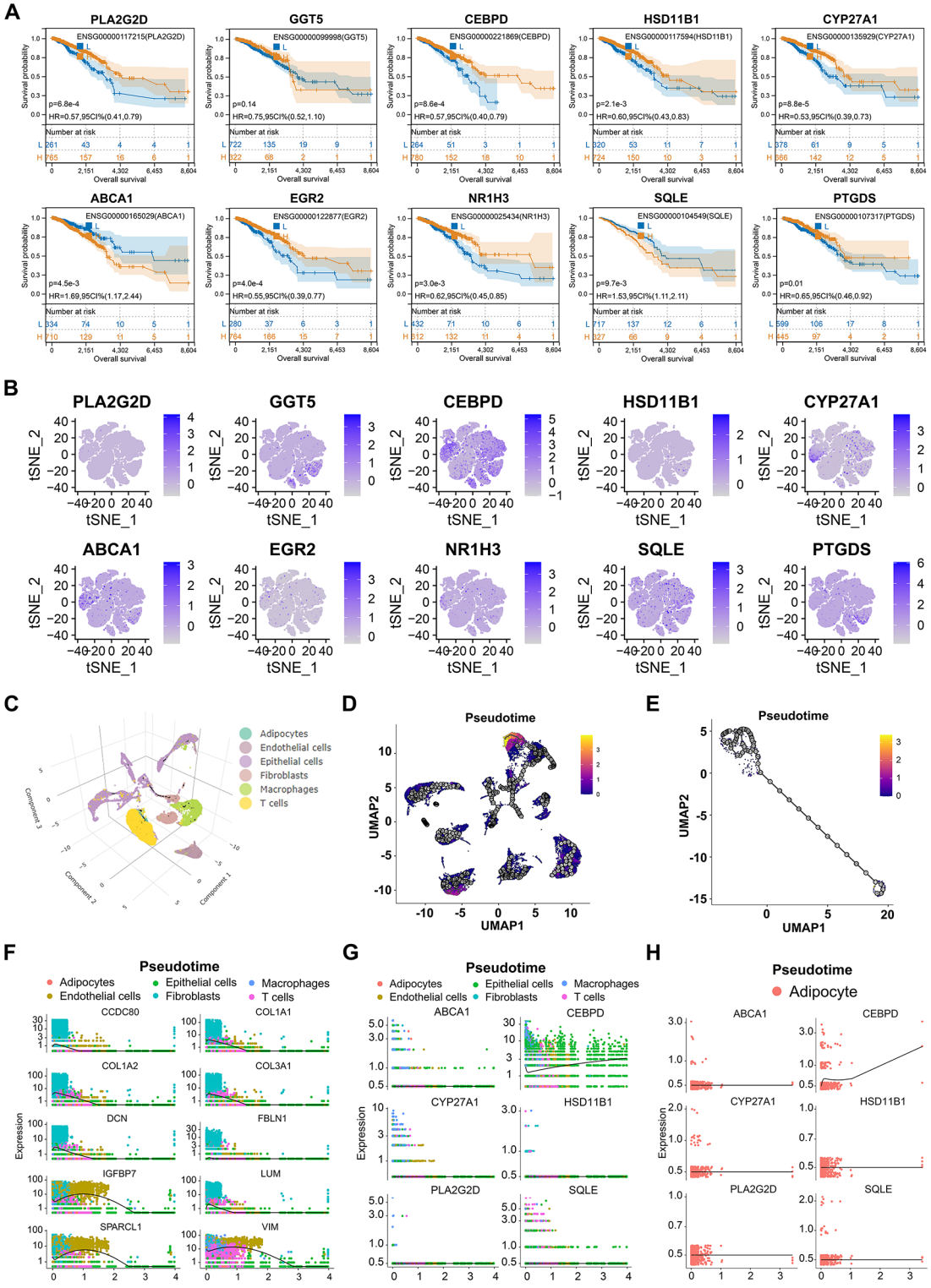

Fig. 5. Prognostic significance and single-cell analysis of risk score genes. (**A**) Kaplan-Meier survival analysis of risk score genes. (**B**) Expression distribution of risk score genes in single-cell t-SNE plots. (**C**) Cell development simulation analysis based on single-cell datasets. (**D**) Pseudo-chronological developmental trajectories of all cells. (**E**) Pseudo-chronological developmental trajectories annotated as adipocytes. (**F**) Top 10 most representative genes in the pseudo-chronological developmental trajectories of all cells. (**G**) Expression changes of risk score genes in the pseudo-chronological developmental trajectories of all cells. (**H**) Expression changes of risk score genes in the pseudo-chronological developmental trajectories annotated as adipocytes.

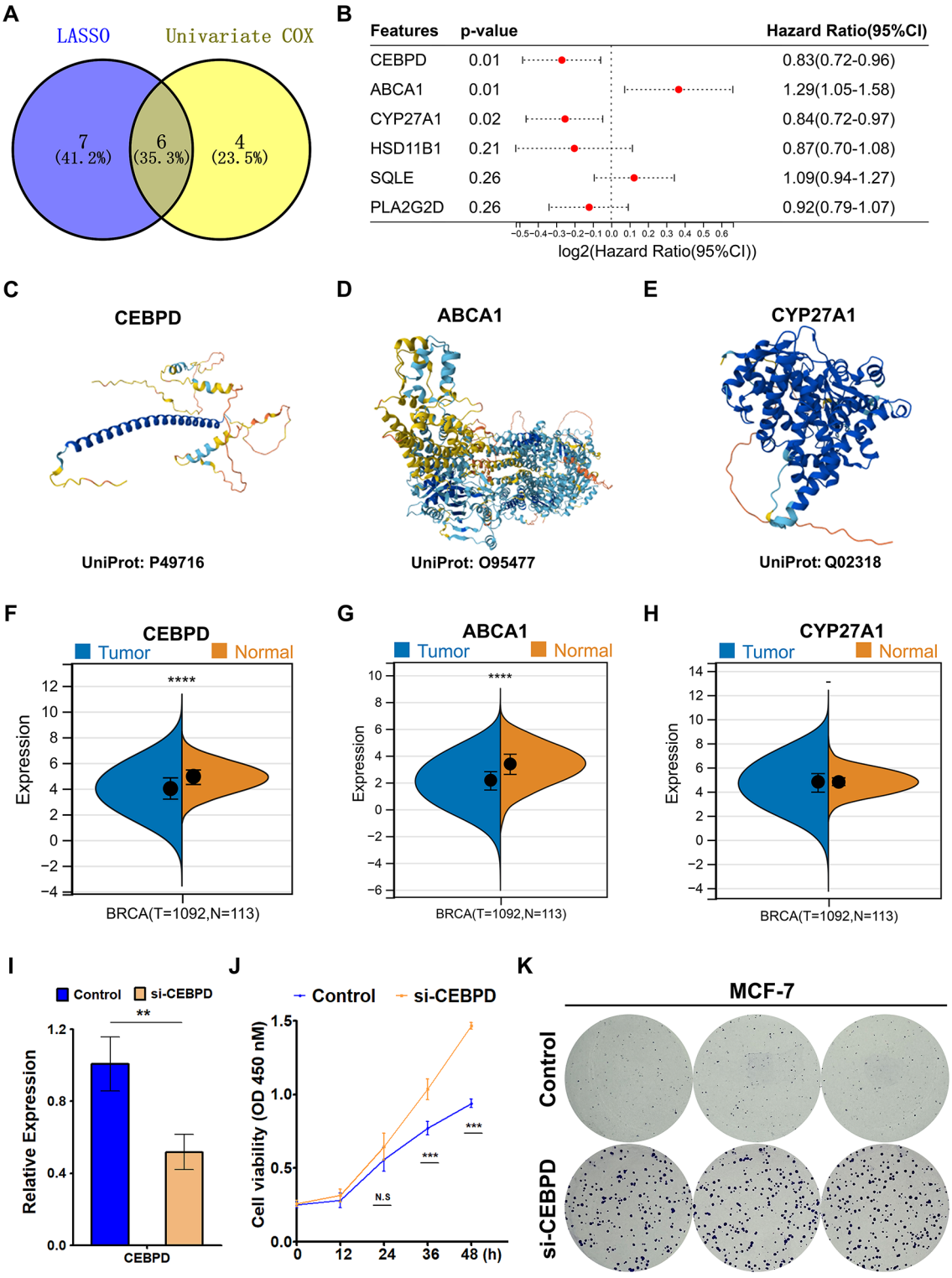

Fig. 6. Screening of the most representative characteristic genes of breast cancer lipid metabolism. (**A**) Venny plot of prognostic analysis scoring genes. (**B**) Multivariate Cox regression analysis of prognostic analysis scoring genes. (**C**) CEBPD protein structure predicted by alphafold. (**D**) ABCA1 protein structure predicted by alphafold. (**E**) CYP27A1 protein structure predicted by alphafold. (**F**) Difference in CEBPD transcription level between normal group and tumor group in TCGA-LIHC cohort. (**G**) Difference in ABCA1 transcription level between normal group and tumor group in TCGA-LIHC cohort. (**H**) Difference in CYP27A1 transcription level between normal group and tumor group in TCGA-LIHC cohort. (**I**) Real-time fluorescence quantitative PCR to detect the inhibitory efficiency of si-CEBPD. (**J**-**K**) CCK-8 (**H**) and colony formation assay (**I**) to detect the effect of si-CEBPD on the proliferation activity of MCF-7 cells.

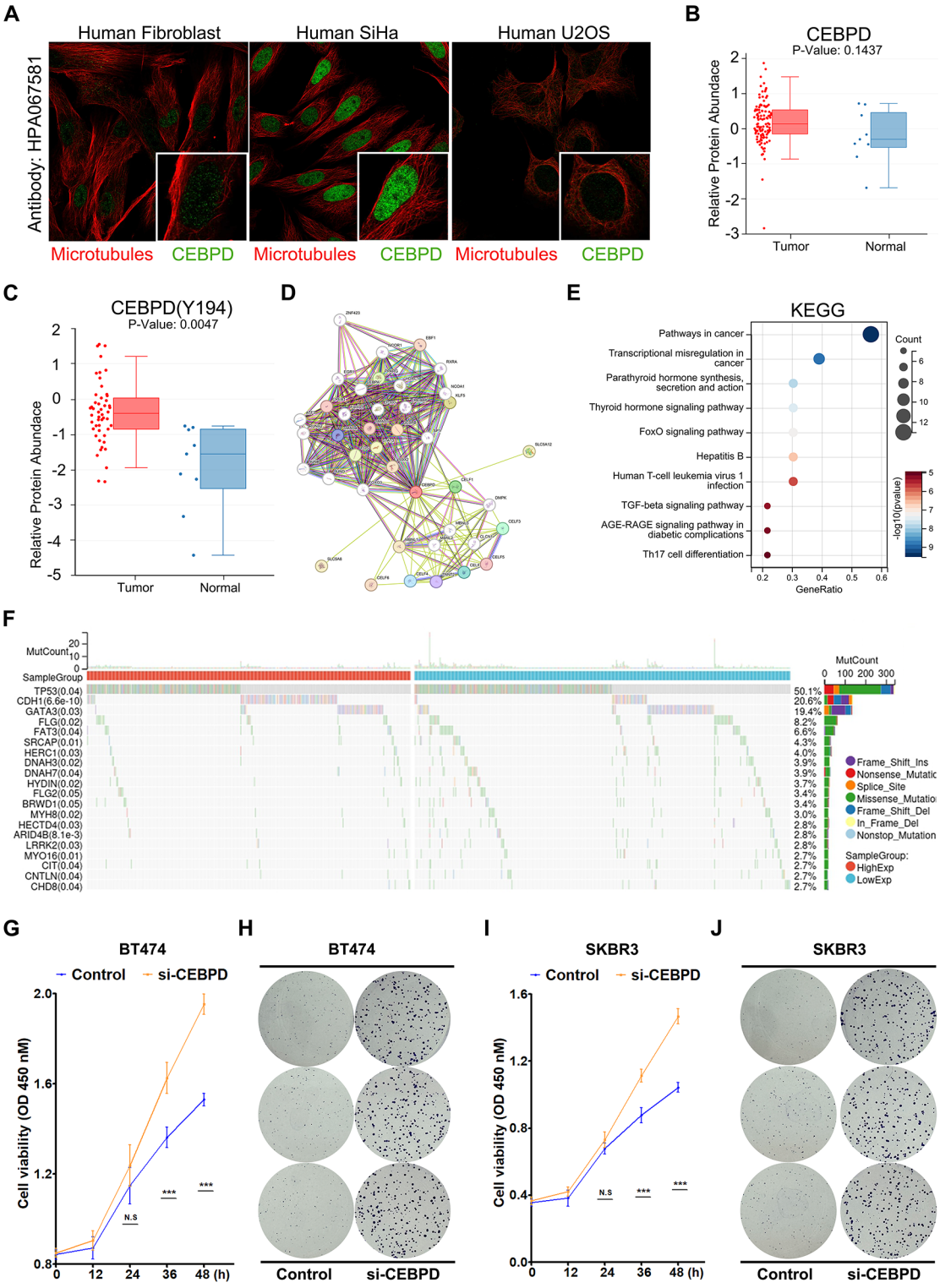

Fig. 7. CEBPD promotes breast cancer cell proliferation and is a reliable lipid metabolism signature prognostic marker. (**A**) Cellular sublocalization of CEBPD in the HPA database. (**B**) Differential expression of CEBPD in normal and tumor tissues in the TCGA proteome cohort. (**C**) Differential expression of CEBPD (Y194) in normal and tumor tissues in the TCGA proteome cohort. (**D**) Protein interaction network of CEBPD in the STRING database. (**E**) KEGG analysis of 40 CEBPD-interacting proteins. (**F**) Mutation analysis of the TCGA-LIHC cohort grouped by CEBPD transcription level. (**G-H**) CCK-8 (**G**) and colony formation assay (**H**) were used to detect the effect of si-CEBPD on the proliferation activity of BT474 cells. (**I,J**) CCK-8 (**I**) and colony formation assay (**J**) were used to detect the effect of si-CEBPD on the proliferation activity of SKBR3 cells.

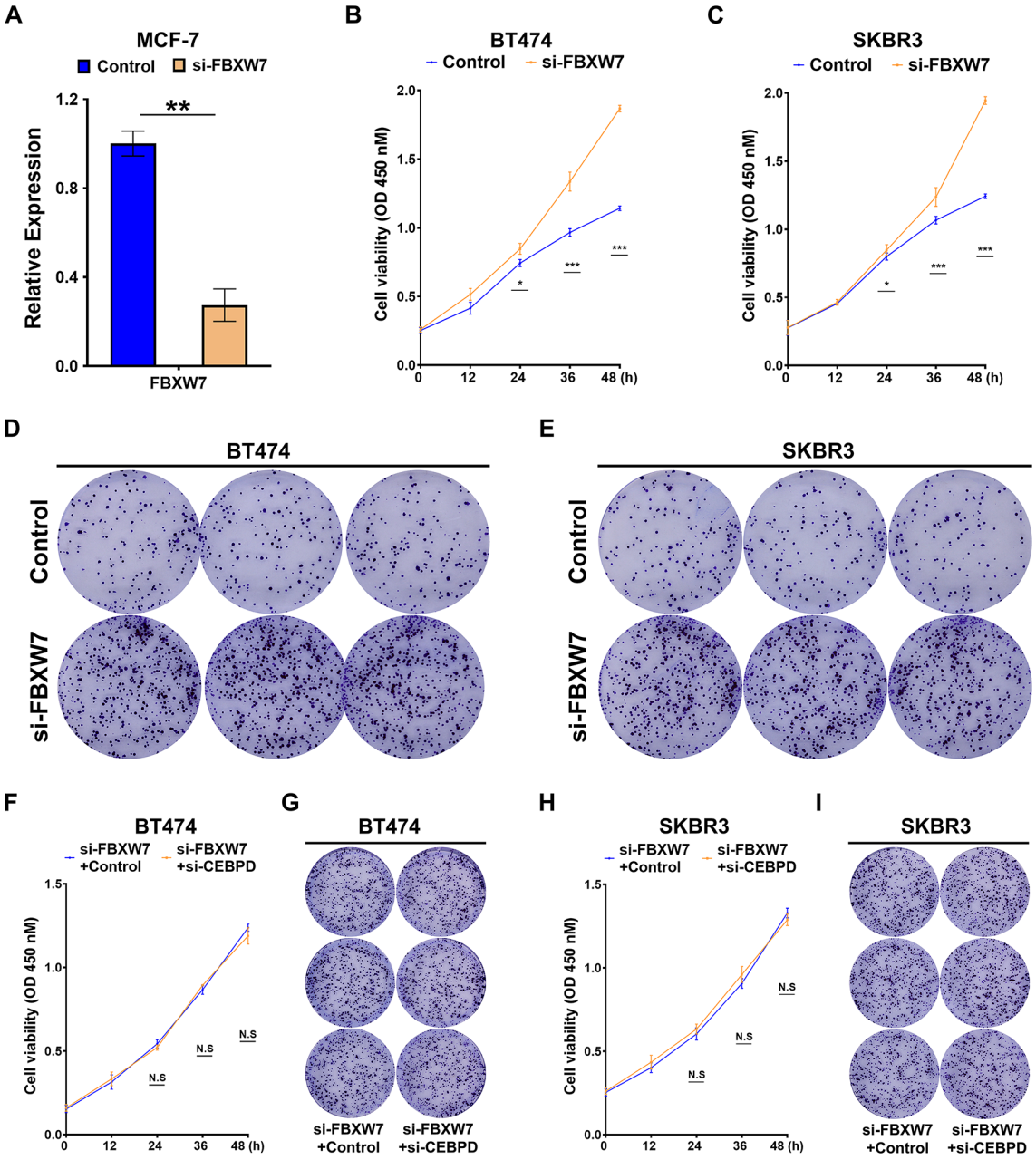

Fig. 8. CEBPD promotes breast cancer cell proliferation in a FBXW7-dependent manner. (**A**) Real-time fluorescence quantitative PCR to detect the inhibitory efficiency of si-FBXW7 in MCF-7 cell. (**B**) CCK-8 were used to detect the effect of si-FBXW7 on the proliferation activity of BT474 cells. (**C**) CCK-8 were used to detect the effect of si-FBXW7 on the proliferation activity of SKBR3 cells. (**D**) Colony formation assay were used to detect the effect of si-FBXW7 on the proliferation activity of BT474 cells. (**E**) Colony formation assay were used to detect the effect of si-FBXW7 on the proliferation activity of SKBR3 cells. (**F**-**G**) CCK-8 (**F**) and colony formation assay (**G**) were used to detect the effect of si-CEBPD on the proliferation activity of BT474 cells based on the inhibition of FBXW7 expression. (**H**-**I**) CCK-8 (**H**) and colony formation assay (**I**) were used to detect the effect of si-CEBPD on the proliferation activity of SKBR3 cells based on the inhibition of FBXW7 expression.

make up the risk score, CEBPD was shown by Kinoshita's group in 1992 to produce transcriptional synergy with NF-IL6[37], playing a crucial role in pathways such as inflammatory response and cell cycle regulation, both of which are associated with cancer progression[37–39]. Evidence suggests that lipid metabolism is considered to play an important role in breast cancer[40–42], which suggests that CEBPD may affect lipid metabolism by regulating genes involved in lipid transport and synthesis, which may affect tumor cell proliferation and immune cell infiltration[43–45]. Our in vitro experiments revealed that inhibition of CEBPD significantly enhanced the proliferation of breast cancer cells, underscoring its potential role as a tumor suppressor[46]. CEBPD is localized

primarily in the nucleus and has been linked to transcriptional regulation and cancer pathways, as shown in our STRING network analysis[47]. Further, mutation analysis revealed that high CEBPD expression is associated with increased mutation frequencies in key cancer-related genes, including CDH1, which is implicated in cell adhesion and metastasis[48]. These results suggest that therapies aimed at enhancing CEBPD activity may offer a new approach to inhibit breast cancer progression, particularly in subtypes with reduced CEBPD expression, such as small molecules or gene editing approaches aimed at restoring its tumor suppressor function.

Our findings also indicate that ABCA1 and CYP27A1 are prognostically significant in breast cancer. Interestingly, while ABCA1 was initially expected to act as a tumor suppressor, its expression was found to correlate with poor prognosis, possibly due to its role in mediating membrane fluidity, which may facilitate cancer cell dissemination[49]. This finding aligns with other studies reporting that ABCA1 overexpression contributes to cancer progression by promoting cholesterol efflux and altering membrane dynamics[50–52]. These findings emphasize the need for precision therapies targeting ABCA1's duality, potentially through selective inhibitors that preserve its physiological roles while mitigating its tumor-promoting effects. Similarly, CYP27A1, involved in cholesterol metabolism, may serve as a target for disrupting metabolic pathways associated with tumor progression. Similarly, CYP27A1, which is involved in cholesterol metabolism, could be explored as a target for disrupting metabolic pathways that promote tumor progression.

Additionally, the immune landscape analysis suggested that a high-risk score, as determined by lipid metabolism gene expression, is associated with altered immune cell infiltration patterns. We observed that high-risk patients exhibited reduced levels of immune cell infiltration, particularly B and T cells, and a corresponding increase in immune evasion markers, such as MDSCs and CAFs. These alterations may contribute to immunosuppression within the tumor microenvironment, providing insights into why high-risk patients have worse outcomes and are less likely to benefit from immunotherapy[53–55]. Clinically, these findings suggest that high-risk patients may exhibit resistance to conventional immunotherapies due to impaired anti-tumor immunity and enhanced immune evasion. Our analysis also revealed that patients in the high-risk group presented with more advanced tumor stages, indicating that lipid metabolism dysregulation may correlate with disease progression and metastatic potential[56,57]. These results suggest that combining immune checkpoint inhibitors with lipid metabolism modulators may enhance immune activation and therapeutic efficacy, particularly in high-risk patients.

This study uniquely identifies CEBPD as a regulator of breast cancer cell proliferation by integrating single-cell transcription and TCGA whole-transcriptome data, starting from lipid metabolism risk characteristics. While not groundbreaking, it consolidates prior findings on CEBPD in breast cancer and highlights lipid metabolism as a promising research avenue for uncovering its roles. Our study, however, has several limitations. For example, this study selected single-cell data from different disease subtypes (triple-negative breast cancer and ER + breast cancer) for combined analysis, which makes the relevant conclusions insufficient in the study of other phenotypes. Although we validated the association of lipid metabolism-related genes with breast cancer prognosis, further studies using larger and more diverse cohorts are needed to confirm these findings and explore potential mechanistic insights[58–60]. Additional in vivo studies are also essential to fully elucidate the functional roles of CEBPD, ABCA1, and CYP27A1 in tumor growth and metastasis.

Conclusion

This study analyzed adipocyte and lipid metabolism signature genes in breast cancer, highlighting the complex interactions between adipocytes and the tumor immune microenvironment. Functional experiments demonstrated that CEBPD, identified as a lipid metabolism-associated prognostic gene, has the potential to inhibit cell proliferation. These findings lay the foundation for developing targeted therapies that exploit metabolic vulnerabilities in breast cancer cells, ultimately aiming to improve patient prognosis.

Data availability

The datasets presented in this study can be found in the GEO (GENE EXPRESSION OMNIBUS) online repository under accession numbers GSE263995 and GSE248288 (https://www.ncbi.nlm.nih.gov/). Bulk-RNA data of breast cancer are from the TCGA project (https://portal.gdc.cancer.gov/, accessed September 9, 2024). All publ icly available data are fully described in the Methods section. In addition, all data generated or analyzed during this study are included in this published article.

Received: 20 November 2024; Accepted: 17 February 2025
Published online: 24 February 2025

References

1. Harris, M. A. et al. Towards targeting the breast cancer immune microenvironment. *Nat. Rev. Cancer*. **24** (8), 554–577 (2024).
2. Waks, A. G. & Winer, E. P. Breast Cancer treatment: A review. *JAMA* **321** (3), 288–300 (2019).
3. Trapani, D. et al. Global challenges and policy solutions in breast cancer control. *Cancer Treat. Rev.* **104**, 102339 (2022).
4. Wu, Q. et al. Cancer-associated adipocytes: key players in breast cancer progression. *J. Hematol. Oncol.* **12** (1), 95 (2019).
5. Zhou, X. et al. The pleiotropic roles of adipocyte secretome in remodeling breast cancer. *J. Exp. Clin. Cancer Res.* **41** (1), 203 (2022).
6. Ishay-Ronen, D. & Christofori, G. Targeting Cancer cell metastasis by converting Cancer cells into fat. *Cancer Res.* **79** (21), 5471–5475 (2019).
7. Herrera-Vargas, A. K. et al. Pro-angiogenic activity and vasculogenic mimicry in the tumor microenvironment by leptin in cancer. *Cytokine Growth Factor. Rev.* **62**, 23–41 (2021).
8. Addala, V. et al. Computational Immunogenomic approaches to predict response to cancer immunotherapies. *Nat. Rev. Clin. Oncol.* **21** (1), 28–46 (2024).
9. Tirosh, I. & Suva, M. L. Cancer cell States: lessons from ten years of single-cell RNA-sequencing of human tumors. *Cancer Cell.* **42** (9), 1497–1506 (2024).

10. Kundu, M. et al. Modulation of the tumor microenvironment and mechanism of immunotherapy-based drug resistance in breast cancer. *Mol. Cancer*. **23** (1), 92 (2024).
11. Liu, Y. M. et al. Combined Single-Cell and Spatial transcriptomics reveal the metabolic evolvement of breast Cancer during early dissemination. *Adv. Sci. (Weinh)*. **10** (6), e2205395 (2023).
12. Yu, T. J. et al. Bulk and single-cell transcriptome profiling reveal the metabolic heterogeneity in human breast cancers. *Mol. Ther.* **29** (7), 2350–2365 (2021).
13. Li, Y. Q. et al. RARRES2 regulates lipid metabolic reprogramming to mediate the development of brain metastasis in triple negative breast cancer. *Mil Med. Res.* **10** (1), 34 (2023).
14. Ding, J. H. et al. Guanosine diphosphate-mannose suppresses homologous recombination repair and potentiates antitumor immunity in triple-negative breast cancer. *Sci. Transl Med.* **16** (728), eadg7740 (2024).
15. Jin, H. et al. YTHDF2 favors protumoral macrophage polarization and implies poor survival outcomes in triple negative breast cancer. *iScience* **27** (6), 109902 (2024).
16. Tan, J., Egelston, C. A., Guo, W., Stark, J. M. & Lee, P. P. STING signalling compensates for low tumour mutation burden to drive anti-tumour immunity. *EBioMedicine* **101**, 105035 (2024).
17. Butler, A., Hoffman, P., Smibert, P., Papalexi, E. & Satija, R. Integrating single-cell transcriptomic data across different conditions, technologies, and species. *Nat. Biotechnol.* **36** (5), 411–420 (2018).
18. Aran, D. et al. Reference-based analysis of lung single-cell sequencing reveals a transitional profibrotic macrophage. *Nat. Immunol.* **20** (2), 163–172 (2019).
19. Jin, S. et al. Inference and analysis of cell-cell communication using cellchat. *Nat. Commun.* **12** (1), 1088 (2021).
20. Cao, J. et al. The single-cell transcriptional landscape of mammalian organogenesis. *Nature* **566** (7745), 496–502 (2019).
21. Dennis, G. Jr. et al. DAVID: database for annotation, visualization, and integrated discovery. *Genome Biol.* **4** (5), P3 (2003).
22. Kanehisa, M., Furumichi, M., Sato, Y., Kawashima, M. & Ishiguro-Watanabe, M. KEGG for taxonomy-based analysis of pathways and genomes. *Nucleic Acids Res.* **51** (D1), D587–D92 (2023).
23. Szklarczyk, D. et al. The STRING database in 2023: protein-protein association networks and functional enrichment analyses for any sequenced genome of interest. *Nucleic Acids Res.* **51** (D1), D638–D46 (2023).
24. Chen, B., Khodadoust, M. S., Liu, C. L., Newman, A. M. & Alizadeh, A. A. Profiling tumor infiltrating immune cells with CIBERSORT. *Methods Mol. Biol.* **1711**, 243–259 (2018).
25. Racle, J. & Gfeller, D. EPIC: A tool to estimate the proportions of different cell types from bulk gene expression data. *Methods Mol. Biol.* **2120**, 233–248 (2020).
26. Li, D., Rorden, C. & Karnath, H. O. Nonspatial attentional deficits interact with Spatial position in neglect. *J. Cogn. Neurosci.* **29** (5), 911–918 (2017).
27. Luo, J., Chen, J. & He, L. mir-129-5p attenuates Irradiation-Induced autophagy and decreases radioresistance of breast Cancer cells by targeting HMGB1. *Med. Sci. Monit.* **21**, 4122–4129 (2015).
28. Shao, F. L., Liu, Q. Q. & Wang, S. Identify potential miRNA-mRNA regulatory networks contributing to high-risk neuroblastoma. *Invest. New. Drugs*. **39** (4), 901–913 (2021).
29. Shao, F. et al. HPGDS is a novel prognostic marker associated with lipid metabolism and aggressiveness in lung adenocarcinoma. *Front. Oncol.* **12**, 894485 (2022).
30. Wang, Y. et al. NNMT contributes to high metastasis of triple negative breast cancer by enhancing PP2A/MEK/ERK/c-Jun/ABCA1 pathway mediated membrane fluidity. *Cancer Lett.* **547**, 215884 (2022).
31. Balamurugan, K. et al. The tumour suppressor C/EBPdelta inhibits FBXW7 expression and promotes mammary tumour metastasis. *EMBO J.* **29** (24), 4106–4117 (2010).
32. Chen, S., Leng, P., Guo, J. & Zhou, H. FBXW7 in breast cancer: mechanism of action and therapeutic potential. *J. Exp. Clin. Cancer Res.* **42** (1), 226 (2023).
33. Jiang, M. et al. Immunometabolism characteristics and a potential prognostic risk model associated with TP53 mutations in breast cancer. *Front. Immunol.* **13**, 946468 (2022).
34. Shen, L. et al. Exploration of prognosis and immunometabolism landscapes in ER + breast cancer based on a novel lipid metabolism-related signature. *Front. Immunol.* **14**, 1199465 (2023).
35. Cui, H. et al. Comprehensive analysis of nicotinamide metabolism-related signature for predicting prognosis and immunotherapy response in breast cancer. *Front. Immunol.* **14**, 1145552 (2023).
36. Shen, C. et al. Identification and validation of a dysregulated TME-related gene signature for predicting prognosis, and immunological properties in bladder cancer. *Front. Immunol.* **14**, 1213947 (2023).
37. Kinoshita, S., Akira, S. & Kishimoto, T. A member of the C/EBP family, NF-IL6 beta, forms a heterodimer and transcriptionally synergizes with NF-IL6. *Proc. Natl. Acad. Sci. U S A*. **89** (4), 1473–1476 (1992).
38. Bechara, R. et al. The m(6)A reader IMP2 directs autoimmune inflammation through an IL-17- and TNFalpha-dependent C/EBP transcription factor axis. *Sci. Immunol.* **6**(61) (2021).
39. Jin, C. et al. Molecular and genetic insights into human ovarian aging from single-nuclei multi-omics analyses. *Nat. Aging* (2024).
40. Xie, Y. et al. Mammary adipocytes protect triple-negative breast cancer cells from ferroptosis. *J. Hematol. Oncol.* **15** (1), 72 (2022).
41. Pham, D. V. & Park, P. H. Adiponectin triggers breast cancer cell death via fatty acid metabolic reprogramming. *J. Exp. Clin. Cancer Res.* **41** (1), 9 (2022).
42. His, M., Gunter, M. J., Keski-Rahkonen, P. & Rinaldi, S. Application of metabolomics to epidemiologic studies of breast cancer: new perspectives for etiology and prevention. *J. Clin. Oncol.* **42** (1), 103–115 (2024).
43. Banerjee, S. et al. Loss of C/EBPdelta enhances IR-induced cell death by promoting oxidative stress and mitochondrial dysfunction. *Free Radic Biol. Med.* **99**, 296–307 (2016).
44. Lai, H. Y. et al. CCAAT/enhancer-binding protein delta promotes intracellular lipid accumulation in M1 macrophages of vascular lesions. *Cardiovasc. Res.* **113** (11), 1376–1388 (2017).
45. Mason, R. J. et al. Keratinocyte growth factor and the transcription factors C/EBP alpha, C/EBP delta, and SREBP-1c regulate fatty acid synthesis in alveolar type II cells. *J. Clin. Invest.* **112** (2), 244–255 (2003).
46. Hartl, L. et al. CCAAT/Enhancer-Binding protein Delta (C/EBPdelta): A previously unrecognized tumor suppressor that limits the oncogenic potential of pancreatic ductal adenocarcinoma cells. *Cancers (Basel)* **12**(9). (2020).
47. Zhao, Y., Yu, Y., Li, X. & Guo, A. CCAAT enhancer binding protein delta activates vesicle associated membrane protein 3 transcription to enhance chemoresistance and extracellular PD-L1 expression in triple-negative breast cancer. *J. Exp. Clin. Cancer Res.* **43** (1), 115 (2024).
48. Stover, D. G. et al. Association of Cell-Free DNA tumor fraction and somatic copy number alterations with survival in metastatic Triple-Negative breast Cancer. *J. Clin. Oncol.* **36** (6), 543–553 (2018).
49. Plummer-Medeiros, A. M., Culbertson, A. T., Morales-Perez, C. L. & Liao, M. Activity and structural dynamics of human ABCA1 in a lipid membrane. *J. Mol. Biol.* **435** (8), 168038 (2023).
50. Liu, X., Lv, M., Zhang, W. & Zhan, Q. Dysregulation of cholesterol metabolism in cancer progression. *Oncogene* **42** (45), 3289–3302 (2023).
51. Goossens, P. et al. Membrane cholesterol efflux drives tumor-Associated macrophage reprogramming and tumor progression. *Cell. Metab.* **29** (6), 1376–1389 (2019). e4.
52. Pasello, M., Giudice, A. M. & Scotlandi, K. The ABC subfamily A transporters: multifaceted players with incipient potentialities in cancer. *Semin Cancer Biol.* **60**, 57–71 (2020).

53. Azizi, E. et al. Single-Cell map of diverse immune phenotypes in the breast tumor microenvironment. *Cell* **174** (5), 1293–1308 (2018). e36.
54. Wagner, J. et al. A Single-Cell atlas of the tumor and immune ecosystem of human breast Cancer. *Cell* **177** (5), 1330–45e18 (2019).
55. Xiang, H. et al. Cancer-Associated fibroblasts promote immunosuppression by inducing ROS-Generating monocytic MDSCs in lung squamous cell carcinoma. *Cancer Immunol. Res.* **8** (4), 436–450 (2020).
56. Wang, G. et al. Lung cancer scRNA-seq and lipidomics reveal aberrant lipid metabolism for early-stage diagnosis. *Sci. Transl Med.* **14** (630), eabk2756 (2022).
57. Yu, W. et al. Contradictory roles of lipid metabolism in immune response within the tumor microenvironment. *J. Hematol. Oncol.* **14** (1), 187 (2021).
58. Tang, F. et al. A pan-cancer single-cell panorama of human natural killer cells. *Cell* **186** (19), 4235–51e20 (2023).
59. Zhang, H. et al. Systematic investigation of mitochondrial transfer between cancer cells and T cells at single-cell resolution. *Cancer Cell.* **41** (10), 1788–1802 (2023). e10.
60. Du, Y. et al. Integration of Pan-Cancer Single-Cell and Spatial transcriptomics reveals stromal cell features and therapeutic targets in tumor microenvironment. *Cancer Res.* **84** (2), 192–210 (2024).

Author contributions

Author Contributions: YZ: Conceptualization, Data curation, Software, Writing – original draft. YZ and HH: Data curation, Methodology, Writing – original draft. HH and LH: Data curation, Writing – original draft. LY: Conceptualization, Project administration, Funding acquisition Writing – review & editing. All authors listed have made a substantial, direct, and intellectual contribution to the work and approved it for publication.

Funding

This research was supported by the Guizhou Province Traditional Chinese Medicine and Ethnic Medicine Science and Technology Research Project (No. QZYY-2023-112); Guizhou Provincial Medical Research Joint Fund Project (2024GZYXKYJJXM0078).

Declarations

Competing interests

The authors declare no competing interests.

Additional information

Correspondence and requests for materials should be addressed to L.Y.

Reprints and permissions information is available at www.nature.com/reprints.

Publisher's note Springer Nature remains neutral with regard to jurisdictional claims in published maps and institutional affiliations.